RSC Advances

PAPER

View Article Online
View Journal | View Issue

Open Access Article. Published on 23 August 2024. Downloaded on 5/22/2026 7:21:13 PM.
This article is licensed under a Creative Commons Attribution-NonCommercial 3.0 Unported Licence.

Check for updates

Cite this: *RSC Adv.*, 2024, **14**, 25472

Theoretical investigation on degradation of $CH{\equiv}CCH_2OH$ by NO_3 radicals in the atmosphere†

Jikang Gao,[a] Meilian Zhao,[b] Yaru Wang,[a] Junchao Liao[a] and Yunju Zhang *[a]

Received 28th May 2024
Accepted 29th June 2024

DOI: 10.1039/d4ra03922j

rsc.li/rsc-advances

A detailed computational investigation is executed on the reaction between NO_3 and $CH{\equiv}CCH_2OH$ at the CCSD(T)/cc-pVTZ//B3LYP/6-311++G(d,p) level. Addition/elimination and H-abstraction mechanisms are found for the NO_3 + $CH{\equiv}CCH_2OH$ reaction, and they could compete with each other. The most feasible addition/elimination pathway through a series of central-C addition, 1,4-H migration to generate intermediates IM1 ($CHCONO_2CH_2OH$) and IM3 ($CH_2CONO_2CH_2O$), and then IM3 directly decompose into product P2 (CH_2CONO_2CHO + H). The dominant H-abstraction pathway is abstracting the H atom of the $-CH_2-$ group to generate h-P1 (CHCCHOH + HNO_3). RRKM-TST theory was used to compute the kinetics and product branching ratios of the NO_3 + $CH{\equiv}CCH_2OH$ reaction at 200–3000 K. The rate constants at 298 K are consistent with the experimental values. The lifetime of $CH{\equiv}CCH_2OH$ is estimated to be 59.72 days at 298 K. The implicit solvent model was used to examine the solvent effect on the total reaction. Based on the quantitative structure–activity relationship (QSAR) model, the toxicity during the degradation process is increased towards fish, and decreased towards daphnia and green algae.

1. Introduction

In recent years, environmental pollution caused by organic pollutants has been of wide concern from all sectors of society. It has a complex origin and diverse formation mechanisms, and is widely present in the atmosphere, soil, and water.[1] In the past few decades, air pollution caused by solid particulate matter (PM) and volatile organic compounds (VOCs) has become a serious environmental problem threatening human health.[2] Volatile organic compounds have the characteristics of toxicity, persistence, or difficult degradation, which have a certain impact on human health and the growth of animals and plants, and have become important organic pollutants in the environment.[3–5] Research has shown that volatile organic compounds are important substances that affect atmospheric environmental pollution and are also important precursors of secondary organic aerosols (SOA).[6] VOCs not only damage the central nervous system, but also carry the risk of carcinogenesis and mutagenesis.[7] Thus, the degradation of VOCs is urgent. The most common oxidants in the atmosphere are mainly reactive free radicals, such as OH and NO_3 radicals and Cl atoms.[8] Nitrate (NO_3) radicals are the main oxidants at night and play an important role in the chemistry of the lower troposphere.[9] The study of its reaction mechanism and reaction kinetics with pollutants in the atmospheric environment is helpful to better understand the atmospheric chemical process and improve the atmospheric environment. At present, the mechanism and kinetics for the reaction of olefins and saturated alcohols induced with OH and NO_3 radicals and Cl atoms have been extensively studied.[10] In 2011, Thanh Lam Nguyen *et al.*[11] studied the reaction mechanism and kinetics of C_2H_4 + NO_3, and calculated that the thermal rate constant and experimental data were the total reaction rate constant. In 2020, Inmaculada Colmenar *et al.*[12] studied the reaction mechanism and kinetic properties of 2-ethoxyethanol with OH and NO_3 radicals and Cl atoms, and determined the reaction rate constants of OH and NO_3 radicals and Cl under specific conditions, and calculated the atmospheric life of 2-ethoxy ethanol and proposed the degradation mechanism as well. In 2021, Inmaculada Aranda *et al.*[13] explored the reaction of 3-ethoxy-1-propanol with Cl, OH and NO_3 in the atmosphere. However, this type of oxidation of alkynes has not been reported. $CH{\equiv}CCH_2OH$, also known as 2-propylene-1-alcohol, is a compound with both alkynyl and hydroxyl functional groups. $CH{\equiv}CCH_2OH$ has been widely used as corrosion inhibitors in industry.[14–16] As an important unsaturated VOC, it has a certain impact on the atmospheric environment and endangers human health. Therefore, the degradation of such air pollutants has become an ongoing concern, although they are widely used as monomers and intermediates in industrial chemicals synthesis. To the best of our knowledge, there have been no theoretical studies concerning the reaction of $CH{\equiv}CCH_2OH$ with NO_3 radicals up to now. According to the current research status of $CH{\equiv}CCH_2OH$, the reaction

[a]*Key Laboratory of Photoinduced Functional Materials, Mianyang Normal University, Mianyang 621000, PR China. E-mail: zhangyj010@nenu.edu.cn; Fax: +86 816 2200819; Tel: +86 816 2200064*

[b]*College of Medical Technology, Chengdu University of Traditional Chinese Medicine, Liutai Avenue, Wenjiang District, Chengdu, PR China*

† Electronic supplementary information (ESI) available. See DOI: https://doi.org/10.1039/d4ra03922j

© 2024 The Author(s). Published by the Royal Society of Chemistry

Open Access Article. Published on 23 August 2024. Downloaded on 5/22/2026 7:21:13 PM. This article is licensed under a Creative Commons Attribution-NonCommercial 3.0 Unported Licence.

mechanisms and the potential energy surface (PES) of the radical with NO_3 are studied by quantum chemistry calculations at the CCSD(T)[17]/cc-pVTZ//B3LYP[18,19]/6-311++G(d,p)[20,21] level of theory, the main contents are as follows: the intermediate substances, transition states and products are identified, and the potential barriers of each reaction step are obtained to evaluate the favorable reaction path. In addition, we have obtained the rate constant of $CH{\equiv}CCH_2OH + NO_3$ at 200–2000 K, including the most important product branches, the values of the calculated rate constants reproduce remarkably well the available experiment data. Meanwhile, the atmospheric fate of $CH{\equiv}CCH_2OH$ are also researched using the same level of theory.[22,23]

2. Quantum chemical methods

The B3LYP method with the 6-311++g(d,p) basis set was applied to optimize the geometries of reactants, products, intermediates and products. Moreover, vibration frequency computations were also implemented to make sure of the presence of intermediates with no imaginary frequency, and transition states with one and only one imaginary frequency. To make sure that the transition states linked with designated intermediate, the intrinsic reaction coordinate (IRC) computations[24,25] were also executed at the same level. The polarizable continuum model (PCM) has been successfully applied to simulate aqueous-phase reactions.[26–28] For the reaction of $CH{\equiv}CCH_2OH$ with the NO_3 radical, the aqueous structures were optimized directly at the B3LYP/6-311++g(d,p) level using the solvent PCM. CCSD(T)/cc-pVTZ method to used to gain more trustworthy relative energies of all the species involved in the NO_3 with $CH{\equiv}CCH_2OH$ reaction in gaseous and aqueous phase reactions. All computations were executed with Gaussian 09 package of program.[29] Rice–Ramsperger–Kassel–Marcus theory and transition-state theory was used to compute the rate constants of the NO_3 with $CH{\equiv}CCH_2OH$ reaction.[30] The eco-toxicity of important intermediates and products are appraised employing the program of ECOSAR developed by USEPA.[31]

3. Results and discussion

The schematic illustration of the reaction starting from IM1 and IM2 are displayed in Fig. 1 and 2. The schematic illustration of the hydrogen abstraction reaction is displayed in Fig. 3. The optimized geometric configuration of all the intermediates, transition states, reactants and all products involved in the $CH{\equiv}CCH_2OH$ with NO_3 reaction are presented in Fig. S1 and S2,† respectively. The potential energy surface (PES) of the $CH{\equiv}CCH_2OH$ with NO_3 reaction are presented in Fig. 4. The gaseous and aqueous structures are highly similar. The Zero Point Energies (ZPE), T_1 diagnostics values, relative energies (ΔE), relative enthalpies (ΔH) and Gibbs free energy (ΔG) in gas and aqueous phase reactions are summarized in Tables S1 and S2.† The harmonic vibrational frequencies, moment of inertia, rotational constants, and numbers of the number of imaginary frequencies involved in this reaction are shown in Table S3.† The Z-matrix Cartesian coordinates of all species found on the PESs are shown in Table S4.† Unless otherwise stated, the geometric parameters and energies used in this work are respective obtained at the B3LYP/6-311++G(d,p) and CCSD(T)//B3LYP levels.

3.1. The addition/elimination mechanisms

The NO_3-initial reaction of $CH{\equiv}CCH_2OH$ generate the rich energy intermediates IM1 ($CHCONO_2CH_2OH$) and IM2 ($CHONO_2CCH_2OH$) when the O atom in NO_3 addition to the central-C and the terminal-C atom of $CH{\equiv}CCH_2OH$, respectively. The involved corresponding transition states are labeled as TS1 and TS2, which are displayed in Fig. 1 and 2. The new generation C–O bonds in TS1 and TS2 are 2.002 Å and 2.047 Å. The energy of TS1 and TS2 are 4.76 and 8.22 kcal mol^{-1} higher than the reactants ($CH{\equiv}CCH_2OH + NO_3$). The exothermicity of IM1 ($CHCONO_2CH_2OH$) and IM2 ($CHONO_2CCH_2OH$) generation at the addition processes are estimated to be 16.77 and 16.45 kcal mol^{-1}. IM1 and IM2 could transform into each other through annular transition state TS3. The free energy barrier of IM1 → TS3 → IM2 and IM2 → TS3 → IM1 are 24.26 and 24.90 kcal mol^{-1}. This conversion process is unimportant owing to the high barrier heights. The internal energies of IM1 and IM2 are 16.05 and 15.85 kcal mol^{-1}, which could generate corresponding products through subsequent unimolecular decomposition and isomerization processes.

IM1 could further directly dissociate to products P1 ($CH_2OH + HCCO + NO_2$) through TS4, which involves the simultaneous breakage of C–C and N–O bonds. The breaking C–C and N–O bonds in TS4 are 2.200 and 1.518 Å. The free energy barrier of IM1 → TS4 → P1 is 35.95 kcal mol^{-1}, which prohibited the occurrence of the reaction. In addition, two internal rearrangement channels have been located for IM1. One is the H atom in –OH group shifting to the C atom of –CH group, generating IM3 ($CH_2CONO_2CH_2O$) through a five-membered-ring TS5. The other isomerization channel of IM1 involves the H atom in $-CH_2OH$ group shifting to the C atom of –CH group, generating IM4 (CH_2CONO_2CHOH) through a four-membered-ring TS6. In TS5 and TS6, the breaking O–H and C–H bonds are 1.205 and 1.392 Å, and the generating C–H bonds are 1.336 and 1.475 Å, respectively. The free energy barriers of IM1 → TS5 → IM3 and IM1 → TS6 → IM4 are 17.60 and 31.80 kcal mol^{-1}. Thus, the isomerization of IM1 to IM3 is better than the isomerization of IM1 to IM4. IM3, with the energy of 26.38 kcal mol^{-1}, could dissociate to products P2 ($CH_2CONO_2CHO + H$) by cleavage the C–H bond through TS7 surmounting the free energy barrier of 22.55 kcal mol^{-1}. Beginning with IM4, two probable reaction scenarios are located. IM4 could respective dissociate N–O bond and C–H bond through TS8 and TS9 to generate products P3 ($CH_2COHCHO + NO_2$) and P2. The free energy barrier of IM4 → TS8 → P3 is 8.50 kcal mol^{-1}, which are 37.59 and 14.05 kcal mol^{-1} lower than that of IM4 → TS9 → P2 and IM3 → TS7 → P2, respectively. However, due to the higher free energy barrier of the isomerization of IM1 to IM4 (31.80 kcal mol^{-1}), the most feasible channel from IM1 is IM1 → IM3 → P2.

As for IM2 ($CHONO_2CCH_2OH$), it could directly dissociate the N–O bond to generate P4 ($CHOCCH_2OH + NO_2$) through

Open Access Article. Published on 23 August 2024. Downloaded on 5/22/2026 7:21:13 PM.
This article is licensed under a Creative Commons Attribution-NonCommercial 3.0 Unported Licence.

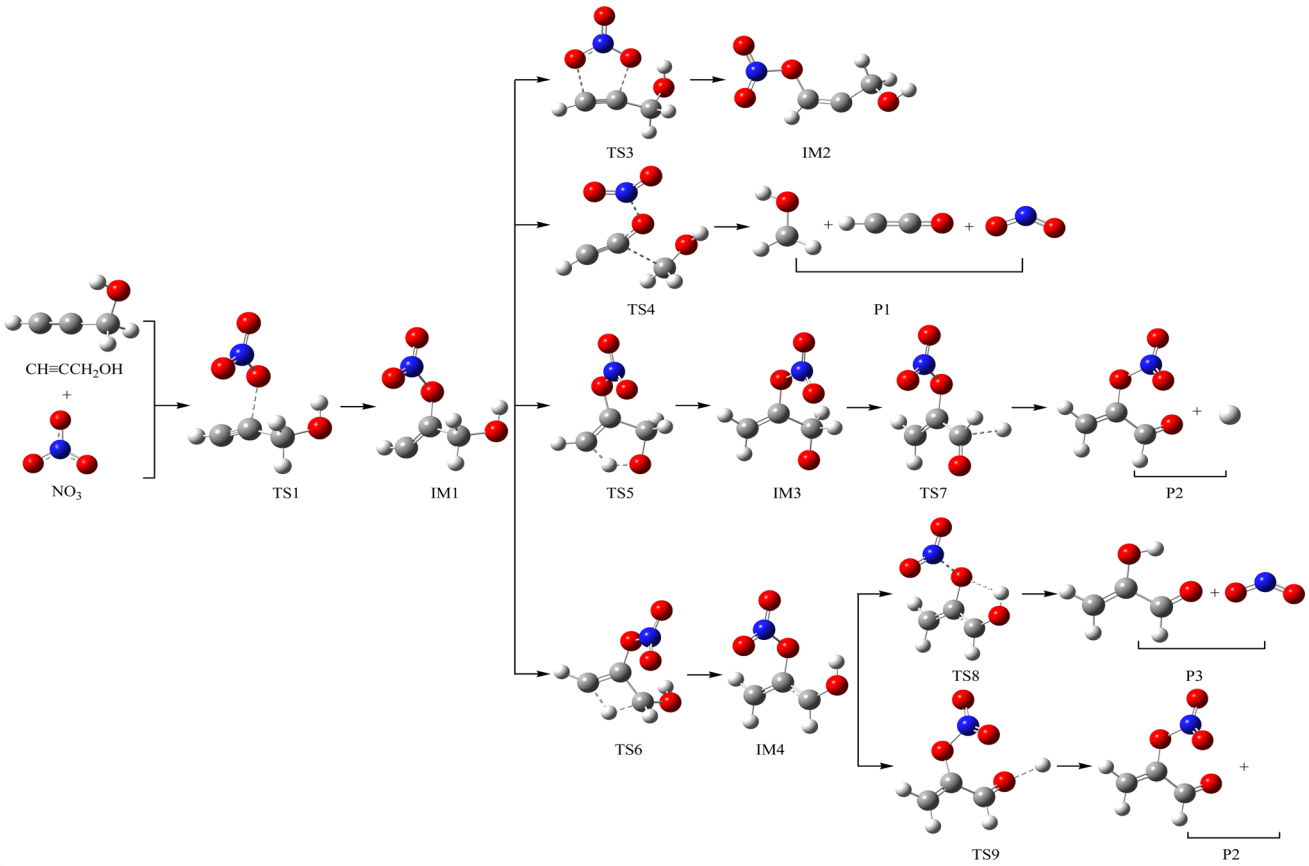

Fig. 1 The schematic illustration of the reaction starting from IM1 in the atmosphere, which obtained at the CCSD//B3LYP level.

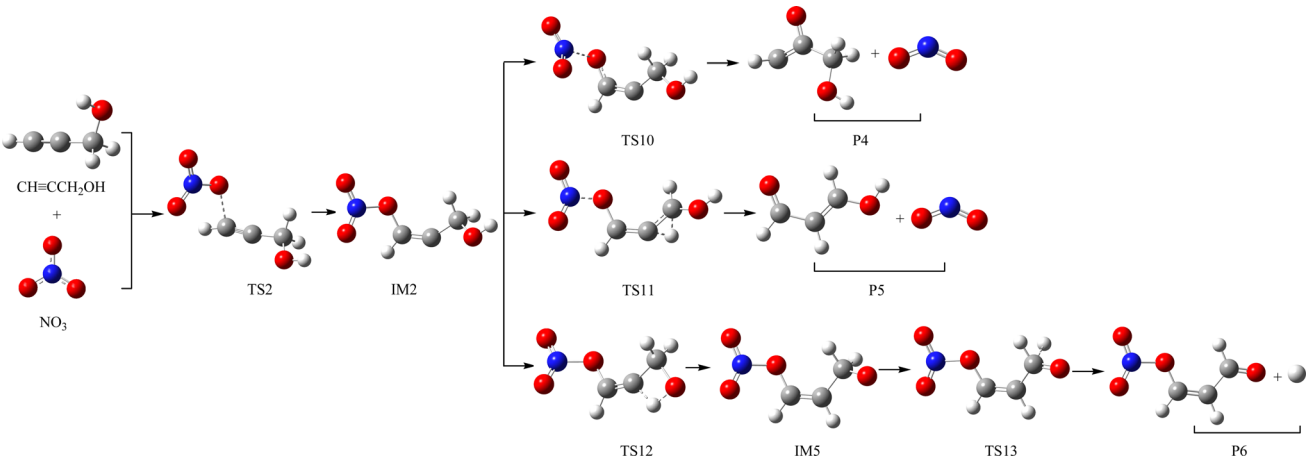

Fig. 2 The schematic illustration of the reaction starting from IM2 in the atmosphere, which obtained at the CCSD//B3LYP level.

TS10 surmounting a free energy barrier of 11.64 kcal mol^{-1}, and this dissociation process is exothermic by 2.84 kcal mol^{-1}. Moreover, P5 (CHOCHCHOH + NO_2) could be generated from IM2 through TS11 involving one of the H atom bonded the C atom of –CH_2OH group shifting to the central-C atom accompanied by breaking the N–O bond. The breaking C–H bond and N–O bond are 1.330 and 1.475 Å, and the new generating C–H bond is 1.326 Å. However, owning to the higher dissociation free energy barrier height (36.72 kcal mol^{-1}), the channel of generating P5 from IM2 is dynamically prohibited. In addition, IM2 could isomerizate to intermediate IM5 ($CHONO_2CHCH_2O$) through TS12 with the alcohol hydrogen shifting to the central-C atom overcoming the free energy barrier of 32.06 kcal mol^{-1}. Subsequently, IM5 undergo simply C–H bond rupture

 © 2024 The Author(s). Published by the Royal Society of Chemistry

Open Access Article. Published on 23 August 2024. Downloaded on 5/22/2026 7:21:13 PM.
This article is licensed under a Creative Commons Attribution-NonCommercial 3.0 Unported Licence.

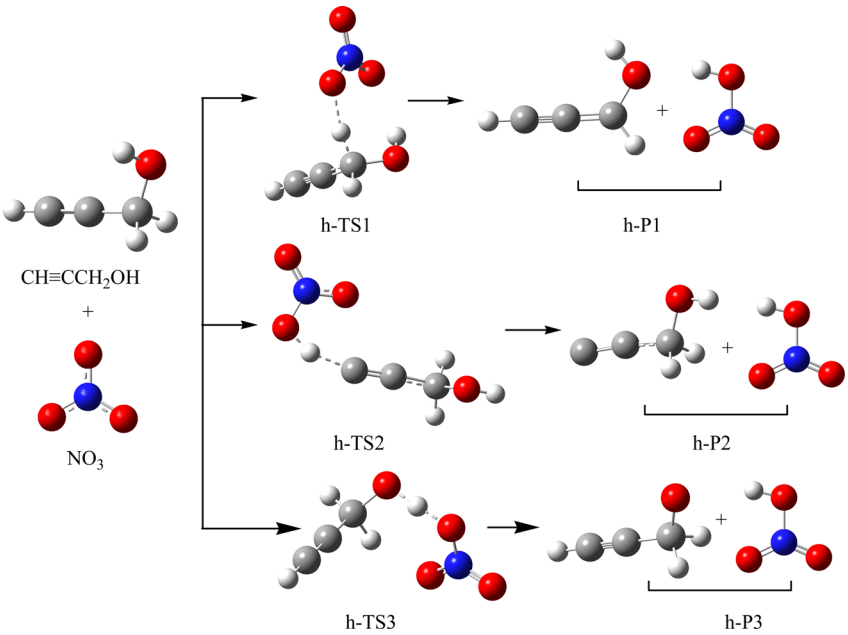

Fig. 3 The schematic illustration of the hydrogen abstraction reaction in the atmosphere, which obtained at the CCSD//B3LYP level.

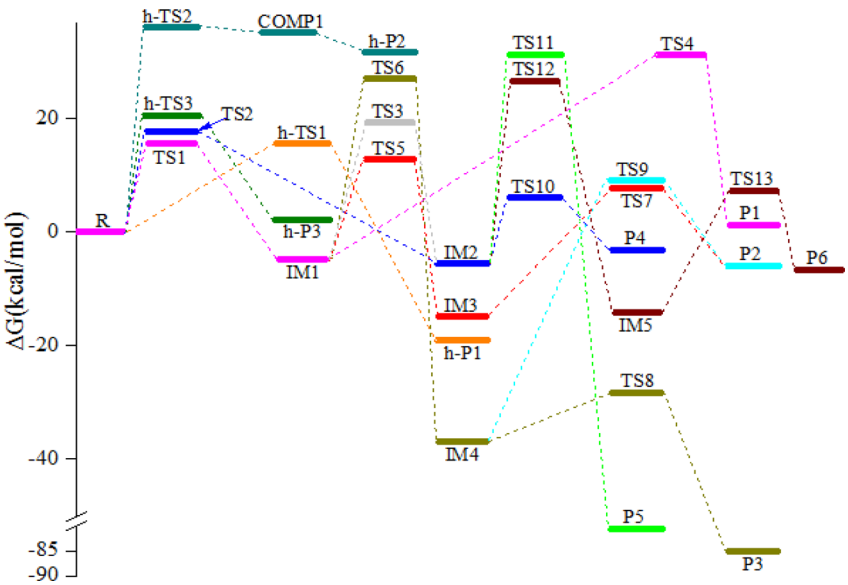

Fig. 4 The potential energy surface (PES) for the NO_3 with $CH{\equiv}CCH_2OH$ reaction in the gas-phase at 298 K.

generating the final products P6 ($CHONO_2CHCHO + H$) through transition state TS13. In TS13, the rupturing C–H bond is 1.828 Å. The free energy barrier of IM5 → TS13 → P6 is 21.22 kcal mol^{-1}. Thus, the pathway of generation of P6 from IM2 contributes less to the reaction.

3.2. The H-abstraction mechanisms

As revealed in Fig. 3 and 4, $CH{\equiv}CCH_2OH$ possesses three different types of H atoms: namely, the H atoms in $-CH_2-$, –CH and –OH group, respectively. OH radical could abstract the H atom from the –CH and $-CH_2-$ group to generate h-P1 ($CHCCHOH + HNO_3$) and h-P2 ($CCCH_2OH + HNO_3$). The corresponding transition states are presented as h-TS1 and h-TS2 in Fig. S1,† respectively. In h-TS1 and h-TS2, the breaking C–H bond are 1.174 and 1.518 Å; and the generating O–H bond are 1.580 and 1.094 Å, respectively. In addition, the OH radical could also abstract the H atom in –OH group through h-TS3. In h-TS3, the breaking and generating O–H bonds are 1.181 and 1.207 Å, respectively. The free energy barrier heights for the above three hydrogen abstraction channels are 15.66, 36.12 and 20.66 kcal mol^{-1}, respectively. Therefore, the most feasible H-abstraction pathway is generation h-P1. Moreover, the free

Open Access Article. Published on 23 August 2024. Downloaded on 5/22/2026 7:21:13 PM.
This article is licensed under a Creative Commons Attribution-NonCommercial 3.0 Unported Licence.

barrier of generation h-P1 is only 0.14 kcal mol^{-1} higher than that of the NO_3 addition to the center-C atom of $CH{\equiv}CCH_2OH$. Hence, the pathway of H-abstraction and addition/elimination could compete with each other.

3.3. The influence of the water environment

The reaction mechanism and advantageous channels of the $CH{\equiv}CCH_2OH$ with NO_3 radical in aqueous solution are the same as those of gaseous reactions under the implicit water model (PCM). It is worth mentioning that, despite our tremendous efforts, transition states TS2 and TS4 were not found. Moreover, the free energy barriers in the gaseous phase are usually lower than those of aqueous reactions except for the processes of IM4 → TS9 → P2, IM2 → TS11 → P5 and IM5 → TS13 → P6. The free energy barriers of IM4 → TS9 → P2, IM2 → TS11 → P5 and IM5 → TS13 → P6 in the aqueous phase are 0.37, 2.39 and 1.18 kcal mol^{-1} lower than those in the

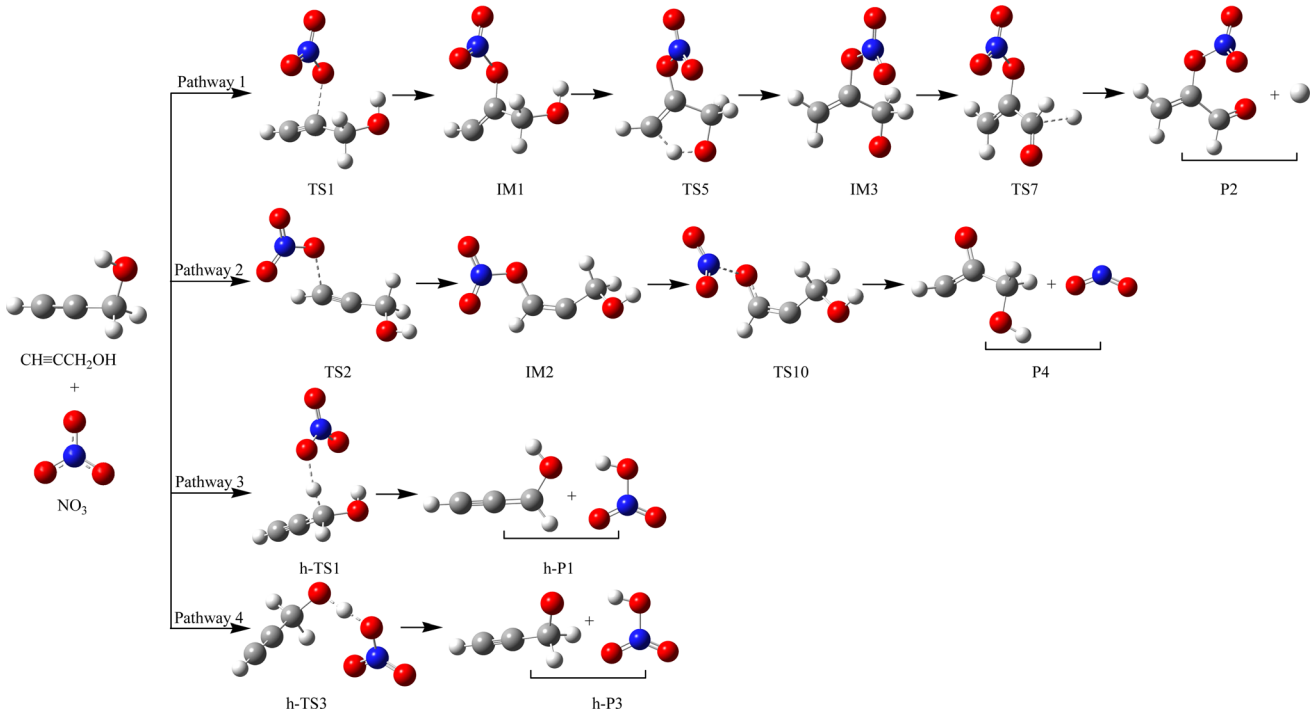

Fig. 5 The dominant reaction pathways using for the dynamic computations.

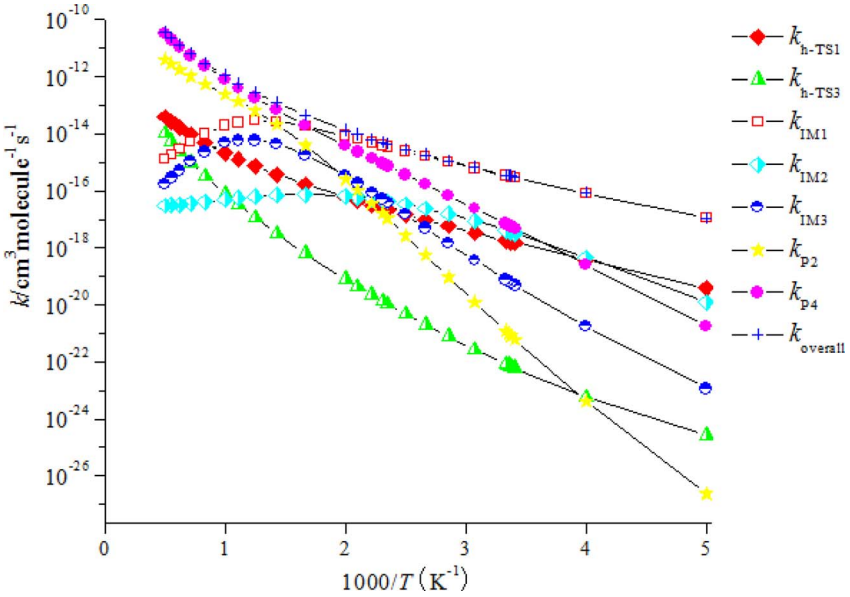

Fig. 6 Temperature dependence of the total and individual rate constants for the NO_3 + $CH{\equiv}CCH_2OH$ reaction at 1 Torr of He, 200–2000 K.

 © 2024 The Author(s). Published by the Royal Society of Chemistry

Open Access Article. Published on 23 August 2024. Downloaded on 5/22/2026 7:21:13 PM.
This article is licensed under a Creative Commons Attribution-NonCommercial 3.0 Unported Licence.

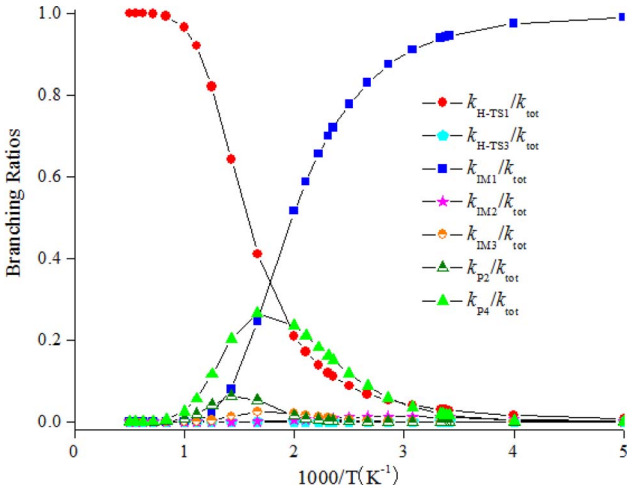

Fig. 7 Branching ratios of the significant product pathways for the NO_3 + $CH{\equiv}CCH_2OH$ reaction at 200–2000 K.

gaseous phase. In addition, the free energy barriers in the gaseous phase for the advantageous channels (R → TS1 → IM1 → TS5 → IM3 → TS7 → P2) are 0.24, 1.12 and 0.12 kcal mol^{-1} lower than those in the aqueous phase, respectively. This result manifested that the water environment has a negative influence on the $CH{\equiv}CCH_2OH$ with NO_3 reaction. Similar phenomena have also been found in some reactions.[32,33]

3.4. The dynamic calculations

To preferably comprehend the fate of $CH{\equiv}CCH_2OH$ in the atmosphere, we used the Fortran program and RRKM theory to compute the rate coefficient of key element reactions (pathways 1–4) at 10 Torr and 298 K. The specifics of the computation process are given in ESI.† The dominant reaction pathways using for the dynamic computations were displayed in Fig. 5.

The computed rate coefficient of the NO_3-initiated reaction of $CH{\equiv}CCH_2OH$ are listed in Table S5.† The temperature dependence of the branching rate coefficients and overall rate coefficients at 200–2000 K are displayed in Fig. 6. Fig. 6 reveals that the rate coefficients for the H-abstraction pathways ($k_{h\text{-}TS1}$ and $k_{h\text{-}TS3}$) and the pathways of generating P2 and P4 (k_{P2} and k_{P4}) present positive temperature dependence. However, the rate coefficients of IM1 ($CHCONO_2CH_2OH$), IM2 ($CHONO_2$-CCH_2OH) and IM3 ($CH_2CONO_2CH_2O$) collisional stabilization channels increase firstly, and then decrease quickly with rising temperatures. The rate constants at 298 K is 3.48×10^{-16} cm^3 per molecule per s. Fig. 7 displayed the branching ratios at the same temperature range and pressure. The low-temperature decomposition is occupied by the generation of IM1 ($CHCONO_2CH_2OH$) at 200–500 K. The channel of generating h-P1 ($CHCCHOH + HNO_3$) through H-abstracting is contribute to the reaction at $T > 500$ K. The generation of the P4 ($CHOCCH_2OH + NO_2$) contribute to the reaction within a certain temperature range. The contribution of other channels to the reaction can be negligible.

3.5. Atmospheric implications of $CH{\equiv}CCH_2OH$

The tropospheric lifetimes (τ) of $CH{\equiv}CCH_2OH$ could be assessed by reacting with NO_3 radicals. The atmospheric lifetimes could be written as:

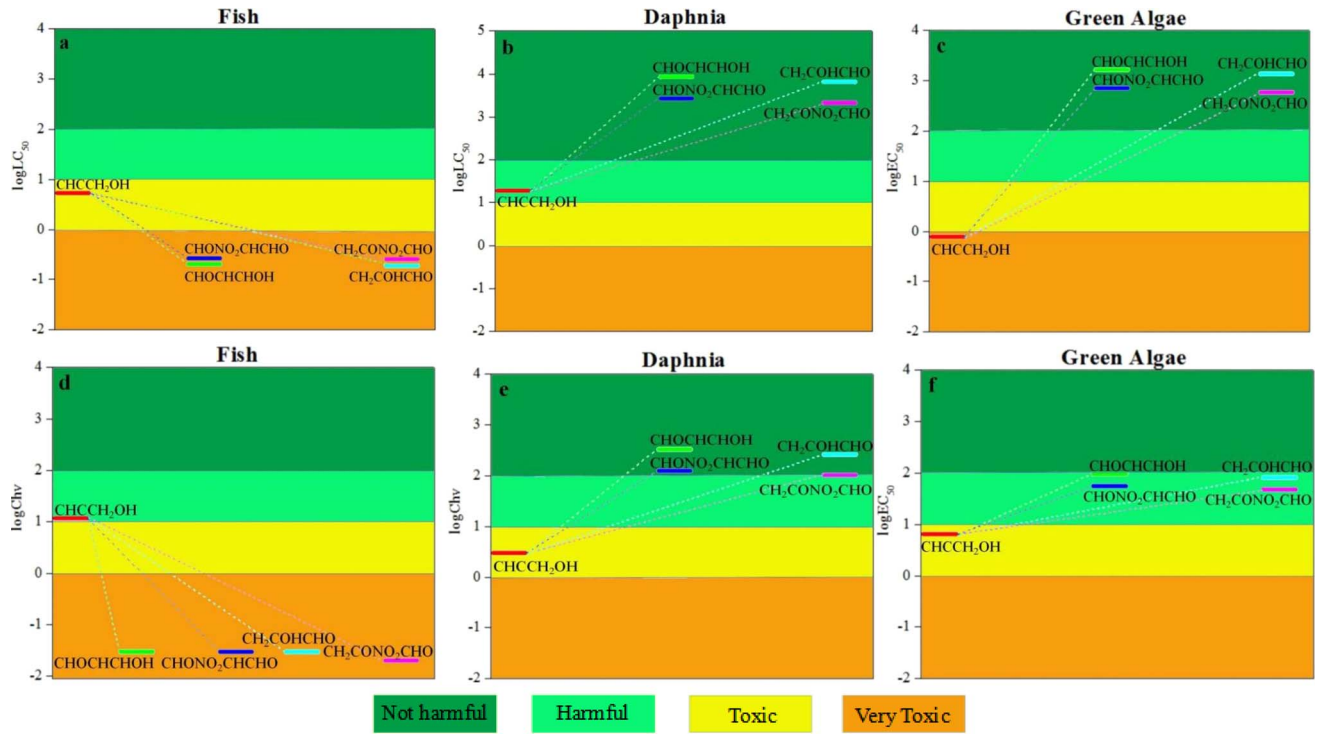

Fig. 8 Acute and chronic toxicity of $CH{\equiv}CCH_2OH$ and its products of the degradation in water to aquatic organisms (mg L^{-1}).

Open Access Article. Published on 23 August 2024. Downloaded on 5/22/2026 7:21:13 PM.
This article is licensed under a Creative Commons Attribution-NonCommercial 3.0 Unported Licence.

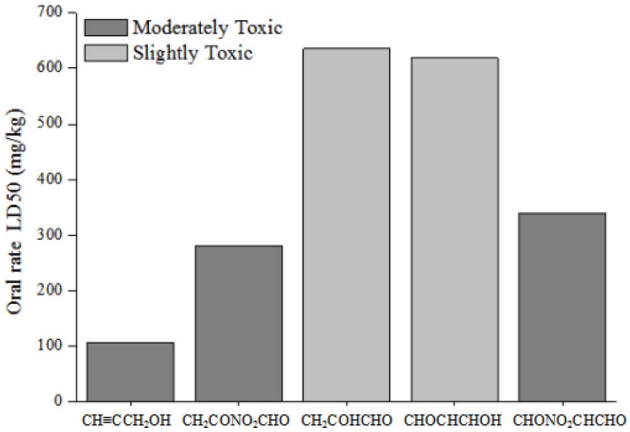

Fig. 9 Oral rate LD_{50} for $CH{\equiv}CCH_2OH$ and its products of the degradation in water.

$$\tau_{NO_3} = \frac{1}{k_{NO_3}[NO_3]}$$

where k_{NO_3} is the rate coefficient of the $CH{\equiv}CCH_2OH$ with NO_3 reaction at 298 K as 3.48×10^{-16} cm^3 per molecule per s. The lifetime of $CH{\equiv}CCH_2OH$ is estimated to be 58.35 days at 298 K using the average atmospheric concentration of NO_3 (5.70×10^8 molecule per cm^3).[34]

3.6. Ecological implications

3.6.1. Acute toxicity and chronic toxicity to aquatic organisms. The computed acute toxicity $\log LC_{50}$ of propargyl alcohol to fish and daphnia and the $\log EC_{50}$ to green algae were 0.73, 1.27 and −0.11 mg L^{-1}, respectively, manifesting that propargyl alcohol is toxic to the three aquatic organisms. As seen from Fig. 8, for fish, the values of $\log LC_{50}$ and $\log Chv$ are negative, manifesting that the toxicity of propargyl alcohol is increased after degradation. For daphnia and green algae, the values of $\log LC_{50}$, $\log EC_{50}$ and $\log Chv$ are larger than of propargyl alcohol, manifesting that the toxicity of propargyl alcohol is diminished after degradation. Furthermore, the order of acute toxicity for the products of the degradation in water (CHOCHCHOH, $CHONO_2CHCHO$, $CH_2COHCHO$ and CH_2CONO_2CHO) were identical to chronic toxicity.

3.6.2. Acute toxicity to rats. The rat (oral) LD_{50} values for propargyl alcohol and its products of the degradation in water are presented in Fig. 9. Obviously, propargyl alcohol, CH_2CONO_2CHO and $CHONO_2CHCHO$ belong to the category of moderately toxic compounds ($50 \leq LD_{50} < 500$ mg L^{-1}). $CH_2COHCHO$ and CHOCHCHOH classify as slightly toxic compounds ($500 \leq LD_{50} < 5000$ mg L^{-1}). As seen from Fig. 9, the toxicity to rats of degradation products of propargyl alcohol are reduced.

3.7. Ecological implications

Apart from researching the toxicity of aquatic organisms and rats of propargyl alcohol and its products of the degradation in water, the evaluation results of developmental toxicity, mutagenicity, and bioaccumulation were forecasted taking advantaging of QSAR method (see Fig. 10). The value of developmental toxicity for propargyl alcohol ($CHCCH_2OH$) is 0.72, which is higher than 0.50. Therefore, $CHONO_2CHCHO$ is developmental toxicant. Similarly, the value of its degradation products in water CH_2CONO_2CHO, $CH_2COHCHO$ and CHOCHCHOH are 0.65, 0.62 and 0.71, and also are developmental toxicants. While the value of degradation products $CHONO_2CHCHO$ is 0.40, which is less than 0.5. Thus, $CHONO_2CHCHO$ is developmental non-toxicant. Meanwhile, $CHCCH_2OH$, CH_2CONO_2CHO, $CHONO_2CHCHO$ are Ames-positive compound (Ames mutagenicity > 0.50: mutagenicity positive). $CH_2COHCHO$ and CHOCHCHOH are Ames-negative compound (Ames mutagenicity < 0.50: mutagenicity negative).

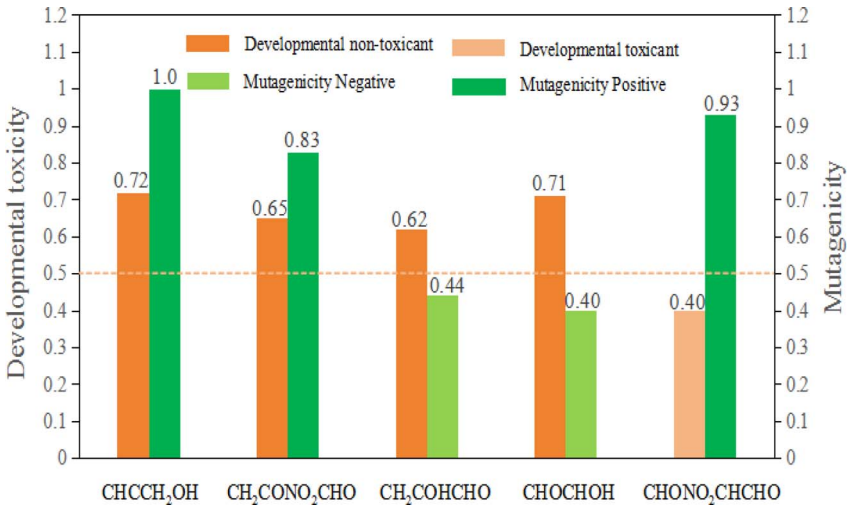

Fig. 10 Oral rate LD_{50} for $CH{\equiv}CCH_2OH$ and its products of the degradation in water.

 © 2024 The Author(s). Published by the Royal Society of Chemistry

Open Access Article. Published on 23 August 2024. Downloaded on 5/22/2026 7:21:13 PM.
This article is licensed under a Creative Commons Attribution-NonCommercial 3.0 Unported Licence.

Thus, except $CH_2COHCHO$ and CHOCHCHOH, the degradation products of propargyl alcohol are harmful to the genes of organisms.

4. Conclusion

The potential energy surface (PES) and mechanism of the NO_3 with $CH{\equiv}CCH_2OH$ reaction has been researched at the CCSD(T)/cc-pVTZ//B3LYP/6-311++G(d,p) level. The rate constants containing the most significant product branches starting from NO_3 + $CH{\equiv}CCH_2OH$ have been gained at 200–2000 K using RRKM-TST theory. The useable experimental dynamic data could be quantitatively reproduced through computations. Addition/elimination and H-abstraction mechanisms have been discovered in the title reaction. IM1 ($CHCONO_2CH_2OH$) are the primary products below 500 K. A significant portion of the NO_3 with $CH{\equiv}CCH_2OH$ reaction produces $CH{\equiv}CCHOH$ and H_2O at T > 500 K. The total rate constants reveal positive temperature dependence at 200–2000 K. Moreover, the calculated rate constants are consistent with the experimental value. The lifetime of $CH{\equiv}CCH_2OH$ is estimated to be 58.35 days at 298 K. Finally, the acute and chronic toxicity of $CH{\equiv}CCH_2OH$ during the degradation process was increased to fish, and decreased to daphnia and green algae based on the QSAR model.

Data availability

The data that support the findings of this study are available on request from the corresponding author.

Author contributions

The conception and design of calculation: Yunju Zhang, Jikang Gao and Meilian Zhao. The execution and analysis of calculation: Yaru Wang and Junchao Liao. Paper writing: Yunju Zhang, Meilian Zhao and Jikang Gao. All authors have reviewed the manuscript.

Conflicts of interest

The authors declare that they have no known competing financial interests or personal relationships that could have appeared to influence the work reported in this paper.

Acknowledgements

This work was supported by the Natural Science Foundations of China (No. 21707062), Scientific Research Starting Foundation of Mianyang Normal University (No. QD2016A007). Sichuan Province Science and Technology Project Support Program (No. 2023NSFSC1119).

References

1 J. H. Zhu, D. S. Liu, C. S. Li, B. J. Zhang, J. L. Wang, W. J. Wu, J. W. Ji and Y. Q. Ma, *RSC Adv.*, 2021, **11**, 35408–35414.
2 Y. W. Feng, L. L. Ling, J. H. Nie, K. Han, X. Y. Chen, Z. F. Bian, H. X. Li and Z. L. Wang, *ACS Nano*, 2017, **11**, 12411–12418.
3 O. Faroon, J. Taylor, N. Roney, M. E. Fransen, S. Bogaczyk and G. Diamond, *Toxicological Profile for Carbon Tetrachloride*, Department of Health and Human Services, Public Health Service Agency for Toxic Substances and Disease Registry, Atlanta, GA, USA, 2005.
4 C. Walgraeve, *Measuring volatile organic compounds and oxygenated polycyclic aromatic hydrocarbons in air: method development and application*, Ghent University, 2012.
5 S. C. Lu, Q. L. Liu, R. Han, M. Guo, J. Q. Shi, C. F. Song, N. Ji, X. B. Lu and D. G. Ma, *J. Environ. Sci.*, 2021, **105**, 184–203.
6 Q. Liu, Y. Gao, W. W Huang, Z. H. Ling, Z. Wang and X. M. Wang, *Atmos. Res.*, 2022, **274**, 106184.
7 P. Nagaraju, S. H. Puttaiah, K. Wantala, *et al.*, *Appl. Water Sci.*, 2020, **10**, 1–15.
8 J. F. Sun, Q. Mu, H. Kimura, V. Murugadoss, M. X. He, W. Du and C. X. Hou, *Adv. Compos. Hybrid Mater.*, 2022, **5**, 627–640.
9 S. Archer-Nicholls, R. Allen, N. L. Abraham, P. T. Griffiths and A. T. Archibald, *Atmos. Chem. Phys.*, 2023, **23**, 5801–5813.
10 C. H. Sun, L. Q. Lv and S. W. Zhang, *Theor. Chem. Acc.*, 2016, **135**, 1–9.
11 T. L. Nguyen, J. Park, K. Lee, K. Song and J. R. Barker, *J. Phys. Chem. A*, 2011, **115**, 4894–4901.
12 I. Colmenar, S. Salgado, P. Martín, I. Aranda, A. Tapia and B. Cabañas, *Atmos. Environ.*, 2020, **224**, 117367.
13 I. Aranda, S. Salgado, P. Martin, F. Villanueva, E. Martinez and B. Cabanas, *Chemosphere*, 2021, **281**, 130755–130764.
14 Y. Feng, K. S. Siow, W. K. Teo and A. K. Hsieh, *Corros. Sci.*, 1999, **41**, 829–852.
15 E. Duwell, *J. Electrochem. Soc.*, 1962, **109**, 1013–1017.
16 B. B. Pati, P. Chatterjee, T. B. Singh and D. D. N. Singh, *Corrosion*, 1990, **46**, 354–359.
17 Y. S. Lee, S. A. Kucharski and R. J. Bartlett, *J. Chem. Phys.*, 1984, **81**, 5906–5912.
18 A. D. Becke, *J. Chem. Phys.*, 1993, **98**, 5648.
19 C. Lee, W. Yang and R. G. Parr, *Phys. Rev. B: Condens. Matter Mater. Phys.*, 1988, **37**, 785–789.
20 R. Krishnan, J. S. Binkley, R. Seeger and J. A. Pople, *J. Chem. Phys.*, 1980, **72**, 650–654.
21 T. Clark, J. Chandrasekhar, G. W. Spitznagel and P. V. R. Schleyer, *J. Comput. Chem.*, 1983, **14**, 294–301.
22 B. Feng, C. H. Sun, W. W. Zhao and S. W. Zhang, *Environ. Sci.: Processes Impacts*, 2020, **22**, 1554–1565.
23 J. T. Ye, F. Y. Bai and X. M. Pan, *Environ. Sci. Pollut. Res.*, 2016, **23**, 23467–23484.
24 C. Gonzalez and H. B. Schlegel, *J. Chem. Phys.*, 1989, **90**, 2154–2161.
25 C. Gonzalez and H. B. Schlegel, *J. Phys. Chem.*, 1990, **94**, 5523–5527.
26 S. Miertuš, E. Scrocco and J. Tomasi, *Chem. Phys.*, 1981, **55**, 117–129.
27 J. Tomasi, B. Mennucci and R. Cammi, *Chem. Rev.*, 2005, **105**, 2999–3094.

Open Access Article. Published on 23 August 2024. Downloaded on 5/22/2026 7:21:13 PM.
This article is licensed under a Creative Commons Attribution-NonCommercial 3.0 Unported Licence.

28 J. Tomasi and M. Persico, *Chem. Rev.*, 1994, **94**, 2027–2094.
29 M. J. Frisch, G. W. Trucks, H. B. Schlegel, P. W. M. Gill, B. G. Johnson, M. A. Robb, J. R. Cheeseman, T. A. Keith, G. A. Petersson, J. A. Pople, *et al.*, *Gaussian 09*, Gaussian Inc., Wallingford, CT, 2009.
30 K. A. Holbrook, M. J. Pilling and S. H. Robertson, *Unimolecular Reactions*, J. Wiley, Chichester, UK, 1996.
31 *ECOSAR v2.0*, **https://www.epa.gov/oppt/newchems/tools/21ecosar.htm**.
32 F. Y. Bai, S. Ni, Y. Z. Tang, X. M. Pan and Z. Zhao, *Phys. Chem. Chem. Phys.*, 2019, **21**, 17378–17392.
33 F. Y. Bai, S. Ni, Y. Ren, Y. Z. Tang, Z. Zhao and X. M. Pan, *J. Hazard. Mater.*, 2020, **386**, 121636.
34 R. Atkinson, *J. Phys. Chem. Ref. Data*, 1991, **20**, 459–507.

 © 2024 The Author(s). Published by the Royal Society of Chemistry